TOWARDS A CONTROL-CENTRIC MODELLING AND SIMULATION-FRAMEWORK FOR HYPERSONIC GLIDE VEHICLES

J. Autenrieb*, N. Fezans*, P. Gruhn†, J. Klevanski†

* DLR, Institute of Flight Systems, Department of Flight Dynamics and Simulation, 38108 Braunschweig,Germany

† DLR, Institute of Aerodynamics and Flow Technology, Department of Supersonic and Hypersonic Technology, 51147 Köln, Germany

Abstract

The German Aerospace Center (DLR) is currently studying and developing different key technologies for the operational implementation of autonomous hypersonic flight systems into different mission scenarios. One configuration type that is of particular interest for civil and military purposes is the hypersonic glide vehicle (HGV) waverider concept. Such HGVs are operating over profoundly widespread flight envelopes and are posing complex flight dynamical characteristics. To enable the development of high-performance flight control systems that can adequately and robustly handle the system dynamics of such vehicles control-centric modeling and simulation environments are required. This paper presents a generic hypersonic glide vehicle concept developed by DLR and the related control-centric simulation architecture. It includes a parameterized analysis framework that allows considering different types of relevant model uncertainties and assessing their impact on the vehicle dynamic behavior and performance. Finally, an overview of chosen flight mechanical characteristics of the generic hypersonic vehicle are presented.

Keywords

Hypersonics; Hypersonic Glide Vehicles; Waverider; Modelling and Simulation; Flight Control; Flight Mechanics

NOMENCLATURE

Symbols

α	Angle of attack	deg
β	Angle of sideslip	deg
χ	Flight path azimuth angle	rad
$\mathscr{C}$,$\mathscr{O}$	Controllability and observability matrices	
ϵ	Emissivity	-
γ	Flight path angle	rad
H	Altitude	m
I	Inertia tensor	kgm^2
κ	Heat-transfer coefficient	-
λ	Eigenvalue	1/sec
L,M,N	External moments in the body axes	Nm
m	Mass	kg
μ	Flight path roll angle	deg
μ	Mean value of a probability distribution	
n_z	Load factor in the body axis z-direction	-
Φ, Θ, Ψ	Euler angles of roll, pitch and yaw	rad
p,q,r	Roll, pitch, yaw rate in the body axes	rad/s
$\dot{q}$	Heat flux	W/m^2
ρ	Freestream density	kg/m^3
R_n	Nose radius	m
R_{Turn}	Turn radius	m
σ	Stefan-Boltzmann constant	W/m^{2}K^2
σ	Standard deviation of a probability distribution	
A,B,C,D	State-space model matrices	
T	Temperature	K
λ, ϕ	Longitude and latitude	rad
$\dot{\chi}$	Turn rate	deg/s
u,v,w	Translational velocities along the x,y,z axes	m/s

doi: 10.25967/550235

X,Y,Z	External forces in the body axes	N

Indices and Subscripts

cmd	Command
K	Inertial frame
meas	Measurement
ref	Reference

Abbreviations

ADACS	Attitude Divert and Control System
FCS	Flight control system
FDS	Flight dynamic simulation
GHGV-2	Generic hypersonic glide vehicle 2
GNC	Guidance, navigation and control
HGV	Hypersonic glide vehicle
LTI	Linear time-invariant
NMFC	Nonlinear model following controller
PDF	Probability density function

1. INTRODUCTION

In the last years, hypersonic glide vehicles (HGV) have been the subject of research and development efforts of both academia and the industry to an increasing extent. This emerging class of vehicles possesses the ability to be applied in the civil and military sectors. One particular area of application that is currently receiving significant attention from the defense industry is the field of hypersonic missile technology.

Well-designed guidance, navigation, and control (GNC) sub-systems are needed, for the mostly autnonmous flight vehicles, to operate successfully in the hypersonic domain. GNC systems are responsible for stabilizing the autonomous vehicle along an online or offline computed path to reach the desired location. Particularly for the application in hypersonic vehicles, the implemented GNC systems need to adequately and robustly handle the complex flight dynamics over highly extended flight envelopes. Especially concerning model uncertainties and complex physical effects during the operation in high Mach number regimes, the applied methods are required to ensure successful mission accomplishments while still compensating inaccurate model assumptions [1]. A generic control-oriented simulation environment for system dynamics simulation is required for the goal-driven development of flight control systems (FCS) in the hypersonic domain. The established simulation framework needs to consider the mathematical models of relevant sub-systems and critical environmental effects, model uncertainties, and disturbances. It further should enable the possibility to evaluate the open/closed-loop system dynamics, the flight dynamics performance, and the control performance of the implemented control laws.

In recent years, the scientific community has shared different approaches and methodologies for the control-centered modeling of hypersonic vehicles. In Ref. [2], Kelkar et al. presented a design tool for the control-centered modeling and analysis of early-stage hypersonic vehicle concepts. In Ref. [3], Keshmiri et al. presented a 6-DOF modeling and analysis approach to aid the design of navigation and control systems of a generic hypersonic vehicle. Further relevant work have a stronger focus on the control-oriented modeling of airbreathing hypersonic vehicles and can be found in the Refs. [4, 5].

This paper presents a control-centered flight dynamics simulation environment designed to aid the design process for hypersonic glide vehicle concepts developed by DLR. The suggested framework simulates the linear/nonlinear model in distinct operating points and over whole missions and all as relevant classified algorithms for a detailed analysis of the flight dynamics and control performance are embedded into the software structure. In the second section of this paper, an overview of a generic hypersonic glide vehicle currently developed by DLR and its mission design is given to the reader. Within the third section, the tools and methods for the aerodynamic and flight dynamical simulation of the vehicle are presented and discussed. After this, a summary of the overall software framework and the implementation of the subsystems is given to the reader. Finally, the system dynamic analysis methodologies intregrated in the software architecture are introduced and different examples of time simulations are used to show the maneuverability and agility performances of the considered HGV.

2. THE DLR GHGV-2 CONCEPT

A multi-disciplinary group of DLR developed the generic hypersonic glide vehicle 2 (GHGV-2). The current research project investigates the different technologies for hypersonic glide vehicles, studies, evaluates, and compares physical limitations and performances.

The developed vehicle is shown in Fig. 1a in an overall view and in Fig. 1b in a sectional view with relevant sub-systems, such as the thermal protection system (TPS), guidance, navigation & control system (GNC), battery, and actuators. The flight vehicle concept is grounded on the aerodynamical foundations of waveriders and is designed to improve lift-to-drag ratios within operations in high Mach number regimes [6]. For the aerodynamical control of the system while operating within endoatmospheric altitudes, the vehicle uses a set of integrated fins as control effectors. Four flaps are integrated into the system, two on the upper- and two on the lower side of the vehicle. Concerning the operations in exoatmospheric altitude, where low air density leads to a loss of aerodynamical con-

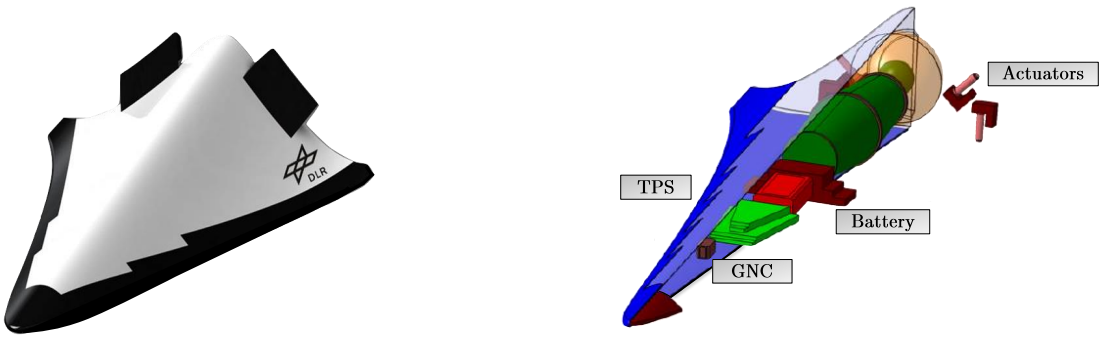

(a) External view on the GHGV-2 **(b) Sectional view of the GHGV-2**

FIG 1. The DLR Generic Hypersonic Glide Vehicle Concept [6].

trol authority, an attitude divert and control system (ADACS) with small propulsors is integrated to generate the needed moments for attitude changes. As this description suggests, the control effectiveness of the implemented control effectors is highly dependent of the vehicle's current flight phase. Since the developed flight control system is focusing on pure attitude control goals (three degrees of freedom) and based on the number of available control effectors in both flight phases (in both cases at least four control effectors), the vehicle can be regarded as over-actuated. For such a system, the application of suitable control allocation algorithms within the later discussed flight control design is required.

DLR developed the presented GHGV-2 concept to study the physical capabilities of strategically used hypersonic glide vehicles and their impact on the perception of hypersonic threats. For the currently investigated use-cases of the GHGV-2, a launch from a two-stage boost-rocket is considered. Within the first boost-phase, the rocket delivers the GHGV-2, which is placed on the head section of the launch vehicle, to an altitude of approximately 100 km. Once that altitude is reached, the HGV decouples from the head section and initiates a free flight period. After the parabolic free flight and a re-entry phase, the HGV enters the atmospheric flight. During this phase the hypersonic system cruises while trying to uphold the $(L/D)_{max}$ related flight path angle γ. This glide phase is carried out within an altitude of approximately 40 km and takes up most of the mission time. FIG. 2 shows that compared to commonly used ballistic missile systems new developed hypersonic operational threats are more challenging to identify and track by earth-based radar systems. Due to the tangentially spreading of the electromagnetic radiation, the lower flying HGV systems are in general later detectable, in comparison as higher flying ballistic missile systems, which leads to significantly shorter reaction times for defense infrastructures after the discovery of an attacking hypersonic glide vehicle. Furthermore, the trajectories and targets of offensively used hypersonic glide systems are more difficult to predict, compared to classical ballistic systems, since HGV possesses higher maneuverability within atmospheric operations.

Within the final flight phase, a hypersonic glide vehicle approaches the defined impact location with a steep and instantaneous negative flight path angle. This final maneuver is often delivered within an inverted flight state for increased pitch maneuverability. During these manouvers it needs to be ensured that a suitable flight speed-altitude matching is guranteed. The flight vehicle is should not possess a Mach number higher than three during such final approach since higher flight velocities combined with higher air densities would damage the structure and, in the worst case, could possibly lead to a burn up of the thermal protection.

3. THE FLIGHT DYNAMIC SIMULATION FRAMEWORK

FIG. 3 presents an high-level overview of the software architecture of the established control-oriented flight dynamics simulation (FDS) framework. The framework is built out of three major processes and modules (simulation control, flight dynamics model, and system dynamics analysis), for which the input-output dependencies are visualized.

The simulation control process is used to allow the user to define which vehicle model from the vehicle data library and which simulation type (complete missions or precise single operating point simulation) shall be used, but also in which flight state the system should be initialized. It is further possible to define the initial vehicle location in the WGS-84 reference ellipsoid and introduce environmental conditions and external disturbances (such as turbulences and gusts) to the simulation. In addition to this, the user can manually update desired parameters and, for example, compare different settings of actuators and sensors within a subsequent system dynamics analysis. Specific functions initialize the generic simulation model using the vehicle data library to obtain the nonlinear or linear flight dynamics model. Once the system is obtained and initialized, it is trimmed (and

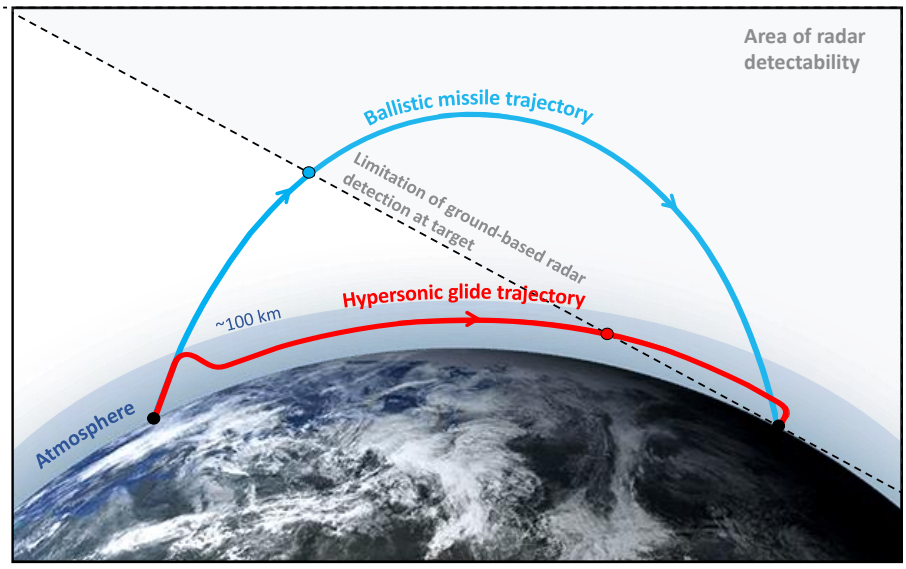

FIG 2. Missions examples and comparisions of HGV and classical Ballistic missile systems.

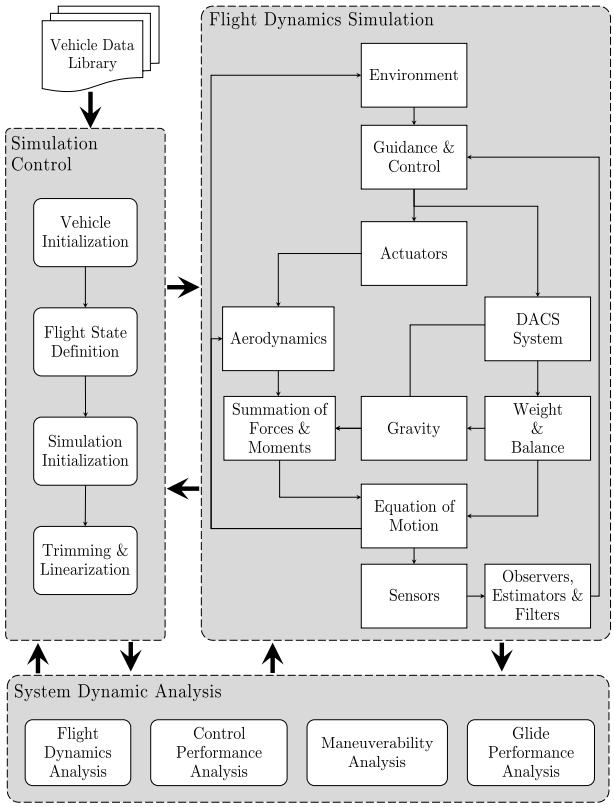

FIG 3. Overall Flight Dynamics Simulation Framework Architecture

if needed linearized) for the ensuing simulation of the defined model.

The proposed simulation model structure is based on the flight dynamics simulation (FDS) framework presented in Ref. [7] and follows a model architecture that is proposed by Hawley et al. in Ref. [8]. The established simulation framework is implemented in MATLAB/Simulink, with additional user-defined functions coded in the C/C++ language as s-functions. The simulation is established for the assistance of the development cycle of different HGV concepts. Since the current system is still under development, the framework was designed to focus on the generalization and parameterization of the simulation model. Most of the subsystems identified as critical on the control performance are considered, modulated, and implemented. This includes actuator and sensors modules. The ADACS systems are currently still under development and hence only an intermediate placeholder module is integrated in the simulation environment, but it is planned to incorporate a full version of the module in furture project steps.

Being able to run detailed analysis routines and workflows to investigate the hypersonic concept is crucial to understand the system dynamics of the aerial vehicle and its performance. The flight dynamics analysis concentrates on the classical aspects of investigations such as the vehicle's stability properties and the analysis of the control effector influences on the balance of moments. The control performance analysis focuses on evaluating the robustness and accuracy of the developed control system in the nominal case and under the presence of parameter uncertainties and control effector failures. The maneuverability and glide-performance analysis is used to indicate crucial vehicle capabilities over the flight envelope and to use the gained knowledge to assist the mission design of the HGV. For all of the described analysis classes, detailed discussions and examples are presented in Sect. 4.

3.1. Aerodynamics

The implemented aerodynamic model accounts for static and dynamic aerodynamics (static coefficients and dynamic derivatives), each formulated as a function of Mach number Ma, altitude H, angle of attack α and angle of sideslip β (Eq. 1- 6). The aerodynamic dataset used for the results presented in this paper employed only the static coefficients for aerodynamic forces (C_A, C_Y, C_N) and moments (C_L, C_M, C_{LN}), and dynamic derivatives have been neglected (set to zero).

$$X = [C_X(\alpha, \beta, \mathrm{Ma}, \mathrm{H}) + C_{X,q}(\alpha, \beta, \mathrm{Ma}, \mathrm{H})\frac{ql_{ref}}{2V}]\frac{\rho}{2}V^2 S_{ref} \tag{1}$$

$$Y = [C_Y(\alpha, \beta, \mathrm{Ma}, \mathrm{H}) + C_{Y,r}(\alpha, \beta, \mathrm{Ma}, \mathrm{H})\frac{rl_{ref}}{2V}] + C_{Y\dot{\beta}}(\alpha, \beta, \mathrm{Ma}, \mathrm{H})\frac{\dot{\beta}l_{ref}}{2V}]\frac{\rho}{2}V^2 S_{ref} \tag{2}$$

$$Z = [C_Z(\alpha, \beta, \mathrm{Ma}, \mathrm{H}) + C_{Z,q}(\alpha, \beta, \mathrm{Ma}, \mathrm{H})\frac{ql_{ref}}{2V} + C_{Z,\dot{\alpha}}(\alpha, \beta, \mathrm{Ma}, \mathrm{H})\frac{\dot{\alpha}l_{ref}}{2V}]\frac{\rho}{2}V^2 S_{ref} \tag{3}$$

$$L = [C_l(\alpha, \beta, \mathrm{Ma}, \mathrm{H}) + C_{l,p}(\alpha, \beta, \mathrm{Ma}, \mathrm{H})\frac{ql_{ref}}{2V}]\frac{\rho}{2}V^2 S_{ref} - Y\Delta z_{cp-cg} - Z\Delta y_{cp-cg} \tag{4}$$

$$M = [C_M(\alpha, \beta, \mathrm{Ma}, \mathrm{H}) + C_{M,q}(\alpha, \beta, \mathrm{Ma}, \mathrm{H})\frac{ql_{ref}}{2V} + C_{M\dot{\alpha}}(\alpha, \beta, \mathrm{Ma}, \mathrm{H})\frac{\dot{\alpha}l_{ref}}{2V}]\frac{\rho}{2}V^2 S_{ref} - Z\Delta x_{cp-cg} + X\Delta z_{cp-cg} \tag{5}$$

$$N = [C_N(\alpha, \beta, \mathrm{Ma}, \mathrm{H}) + C_{N,r}(\alpha, \beta, \mathrm{Ma}, \mathrm{H})\frac{rl_{ref}}{2V} + C_{N,\dot{\beta}}(\alpha, \beta, \mathrm{Ma}, \mathrm{H})\frac{\dot{\beta}l_{ref}}{2V}]\frac{\rho}{2}V^2 S_{ref} + X\Delta y_{cp-cg} + Y\Delta x_{cp-cg} \tag{6}$$

The static aerodynamic coefficients have been calculated by computational fluid dynamics (CFD) with the DLR TAU code [9]. In total, around 800 inviscid calculations have been performed in the Mach number range from 0.6 to 12.5, for angles of attack between -6° and 15°, for angles of sideslip between 0° and 3°, and rudder deflection angles of -20° (upper flap deflected), 0° (flush flaps) and 20° (lower flap deflected). The environmental conditions for each Mach number were based on the atmospheric conditions at a specific altitude taken from a pre-determined trajectory (i.e., no further Reynolds number variation was performed). In order to take viscous effects into account, fully viscous Reynolds-Averaged Navier-Stokes simulations have been performed for selected trajectory points. Those calculations were then used to calculate a viscous correction model that was applied to all data points. The corrected coefficients are then implemented as a lookup table into the FDS framework. As an example, FIG. 4 shows the CFD calculated Mach number distribution around the GHGV-2 at Mach number 12.5.

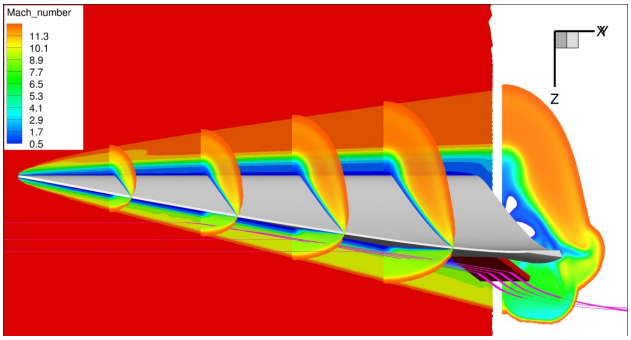

FIG 4. Example image of CFD calculated Mach number distribution around the GHGV-2 at Mach number 12.5

3.2. Flight Dynamic Modulation

Within the established numerical simulation, the motion of the HGV system is described as a generalized second-order differential equation. The implemented nonlinear flight dynamic relationships and the equations of motion are based on classical Newtonian mechanics. The vehicle is assumed as a rigid body, and hence no flexible degrees of freedom are currently considered. FIG. 5 displays the components of the total external forces $(X, Y, Z)^T$, and the total external moments $(L, M, N)^T$ described in the body-fixed-frame.

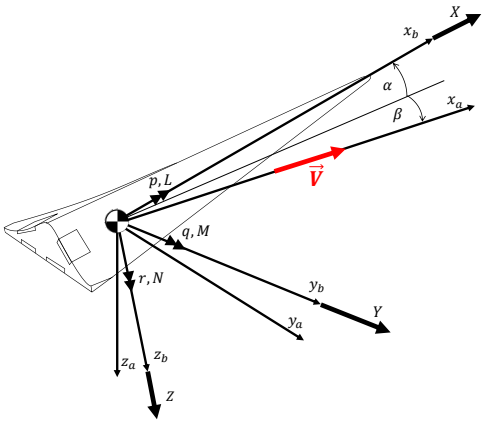

FIG 5. External forces and moments attacking on the GHGV-2 concept

The equations for the translational and rotational movement in the body-fixed frame are presented in Eq. 7 and Eq. 8. The vehicle mass is represented by m, while I is the inertia matrix. The velocity in the body-fixed frame is described with the vector $(u, v, w)^T$.

$$\vec{R} = \begin{bmatrix} X \\ Y \\ Z \end{bmatrix} = m \begin{bmatrix} \dot{u} \\ \dot{v} \\ \dot{w} \end{bmatrix} + m \begin{bmatrix} p \\ q \\ r \end{bmatrix} \times \begin{bmatrix} u \\ v \\ w \end{bmatrix} \tag{7}$$

$$\vec{Q} = \begin{bmatrix} L \\ M \\ N \end{bmatrix} = I \begin{bmatrix} \dot{p} \\ \dot{q} \\ \dot{r} \end{bmatrix} + \begin{bmatrix} p \\ q \\ r \end{bmatrix} \times I \begin{bmatrix} p \\ q \\ r \end{bmatrix} \tag{8}$$

The rotational kinematics between the time derivatives of Euler angles $(\Phi, \Theta, \Psi)^T$ and the body rates are defined as:

$$\begin{bmatrix} \dot{\Phi} \\ \dot{\Theta} \\ \dot{\Psi} \end{bmatrix} = \begin{bmatrix} 1 & \sin\Phi\tan\Theta & \cos\Phi\tan\Theta \\ 0 & \cos\Phi & -\sin\Phi \\ 0 & \frac{\sin\Phi}{\cos\Theta} & \frac{\cos\Phi}{\cos\Theta} \end{bmatrix} \begin{bmatrix} p \\ q \\ r \end{bmatrix} \tag{9}$$

However, in some instances of excessive maneuvers, Euler angles can lead to inconsistencies due to singularities of the geometric computation approaches. To mitigate problems related to those inconsistencies, Quaternions are implemented and can be used if needed. A further kinematic relationship between the flight path roll angle μ, angle-of-attack α and angle of sideslip β, the rotational rates of the vehicle and its flight path conditions can be formulated as given in [10]:

$$\begin{bmatrix} \dot{\mu} \\ \dot{\alpha} \\ \dot{\beta} \end{bmatrix} = \begin{bmatrix} \frac{\cos\alpha}{\cos\beta} & 0 & \frac{\sin\alpha}{\cos\beta} \\ -\cos\alpha\tan\beta & 1 & -\sin\alpha\tan\beta \\ \sin\alpha & 0 & -\cos\alpha \end{bmatrix} \begin{bmatrix} p \\ q \\ r \end{bmatrix} + \begin{bmatrix} \cos\mu\tan\beta & \sin\gamma + sin\mu\tan\beta\cos\gamma \\ -\frac{\cos\mu}{\cos\beta} & -\frac{\sin\mu\cos\gamma}{\cos\beta} \\ -\sin\mu & \cos\mu\cos\gamma \end{bmatrix} \begin{bmatrix} \dot{\gamma} \\ \dot{\chi} \end{bmatrix} \tag{10}$$

The geographical motion of the vehicle is described by the longitude λ, latitude ϕ, and the distance to the earth center R. The kinematic relationship between the flight path and the movement within the modeled WGS-84 reference ellipsoid is defined as given in [11]:

$$\begin{bmatrix} \dot{R} \\ \dot{\lambda} \\ \dot{\phi} \end{bmatrix} = V \begin{bmatrix} \sin\gamma \\ \frac{\sin\chi\cos\gamma}{(R\cos\delta} \\ \frac{\cos\chi\cos\gamma}{R} \end{bmatrix} \tag{11}$$

The aerothermal heating during the re-entry and atmospheric glide phase is a significant and non-trivial influence for analyzing the physical feasibility of a specific mission. Hence it is needed to simulate the attacking heat loads on the vehicle. An approach was chosen that is applicable on the incomplete information basis of the early conceptual design phases but still allows it to consider such influences with sufficient accuracy. The convective heat flux of the stagnation of the vehicle is computed with a Sutton-Graves approach as given in [12].

$$\dot{q} = \kappa\sqrt{\frac{\rho}{R_n}}V^3 \tag{12}$$

In order to compute the temperature at the stagnation point, it is assumed that the convective heat flux instantaneously increases the temperature of the outer skin of the vehicle body. Further it is assumed that the regarded temperature change is directly measurable as a radiative heat flux $\dot{q}$. With these two assumptions, it is possible to balance the two classes of heat flux with the Stefan-Boltzmann law shown in Eq. 13 [13, 14].

$$\dot{q} = \epsilon\sigma T^4 \tag{13}$$

The approach described here, is at the current state, just a simplified and conservative estimation of the occurring heat loads during the simulated maneuvers and missions. Nevertheless, higher quality procedures based on coupled CFD simulations are also used in the project and analyzed separately.

3.3. Flight Control

Especially for HGVs, due to their complex flight physics and coupling effects, the mathematical models might have non-trivial uncertainties, making it challenging to develop reliable, high-performance guidance and control architectures.
A general observation of the flight dynamics of specific hypersonic configurations is that those vehicles tend to an unstable open-loop behavior [15, 16]. In combination with non-minimum phase zeros, this can lead to a significant impact on the closed-loop performance of the flight vehicle.
In recent decades nonlinear control methodologies gained popularity within the scientific community. Those approaches are capable to intrinsically handle the nonlinear system dynamics over the entire flight envelope based on the known mathematical model. Hence, no classical gain-scheduling methodologies are strictly required, even though they can be used to modify the closed-loop behavior for changing operating points. For the GHGV-2, a nonlinear model-following-control (NMFC) method was developed. The structure of the controller is shown in Fig. 6 and is based on the fundamental ideas presented in Ref. [17]. The architecture uses a second-order refer-

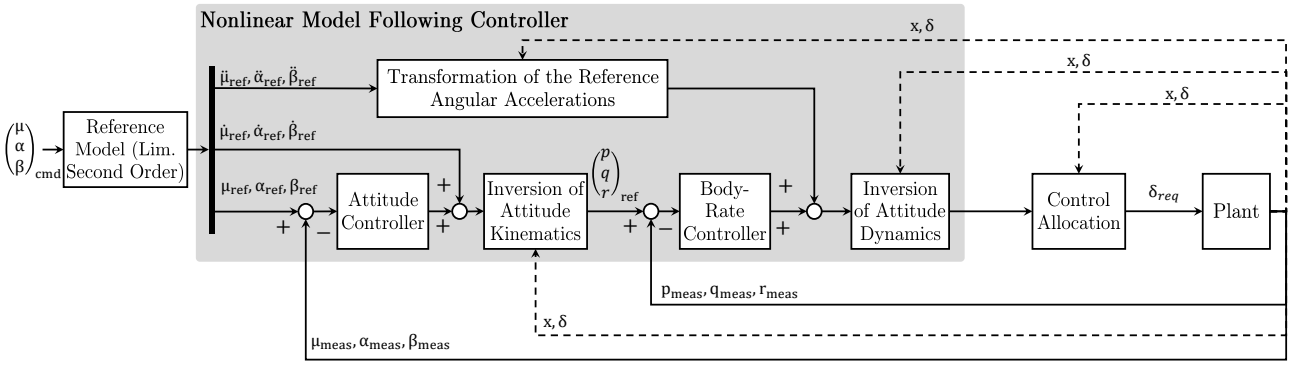

FIG 6. Nonlinear model following control architecture

ence model system to filter the command input vector $(\mu_{cmd}, \alpha_{cmd}, \beta_{cmd})^T$ and shape the desired reference signal vector $(\mu_{ref}, \alpha_{ref}, \beta_{ref})^T$. The generated reference signals are the filtered commands and the corresponding first and second derivatives of the desired model response. The reference model comprises further knowledge of physical limitations on the different time scales and protects the controllers of unworkable reference signals. By using generated feedforward signals, the control task can be mostly decomposed into two main control tasks. The first control task is signal tracking, and the second one is the minimization and regulation of the influences of uncertainties. The first task is mostly carried out by using and transforming the computed feedforward signals based on known systems dynamics. This approach would be already sufficient to command the vehicle for an intrinsically stable system with no uncertainties and in a world with no disturbances. However, since this is not the case for real world scenarios, an additional controller feedback path is needed to handle those influences. The feedback path is based on the idea of a cascaded nonlinear dynamic inversion system presented in Refs. [18, 19]. Since this paper focuses on the modeling aspects of the GHGV-2 project, a detailed discussion about the control architecture would exceed the scope of this publication. Therefore no further information about the control architecture is discussed here, and the authors refer to future publications for detailed discussions about the developed NMFC control system.

4. SYSTEM DYNAMICS ANALYSIS

Before designing a FCS, it is crucial to fully understand the system dynamics over the entire flight envelope. Even after the implementation of the proposed control laws, it is necessary to run detailed analysis routines to investigate the vehicle's flight dynamics and validate the performance of the developed control architecture. For this, advanced analysis methods and workflows need to be embedded into the simulation framework. In Sect. 3, the basic structure of the framework, including a brief introduction of the considered system dynamic analysis categories, were briefly introduced. In this section, more in depth discussions of the system dynamical analysis methods and examples are presented.

4.1. Flight Dynamic Analysis

The majority of the native flight dynamic properties of the hypersonic vehicle are investigated using classical control theory methods based on linear assumptions. Consequently, it is necessary to reduce the complexity of the investigated nonlinear dynamics to the degree of a linear system by linearizing the dynamics around a trimmed operating point. To be able to find a required trim point, a Newton's method-based optimization algorithm is utilized. Once the trim point with the related trim flight state x_0 and the corresponding control input u_0 is found, the system can be linearized. Eq. 14 and Eq. 15 are showing the linear time-invariant (LTI) state-space system, which is commonly used to describe linear flight dynamics.:

$$\dot{x} = Ax(t) + Bu(t) \tag{14}$$

$$y = Cx(t) + Du(t) \tag{15}$$

The stability of the linear flight dynamics can be evaluated by evaluating the eigenvalues by applying the following algebraic method:

$$\left|\lambda I - A\right| = \Delta(\lambda) = (\lambda - \lambda_1)...(\lambda - \lambda_n) \tag{16}$$

If all obtained eigenvalues λ of the system matrix are placed in the left half of the complex plane (negative real part), the linear system can be classified as asymptotic stable. Fig. 7 shows such stability properties of the GHGV-2 at Mach 12.5 and at a constant altitude within the height band of the mesosphere. It can be seen that the system has unstable poles in both the longitudinal and lateral-directional dynamics. Therefore it would not be possible to operate such

a vehicle safely without additional stability augmentation through a FCS.
In order to investigate and visualize the control effectors' influences on the vehicle's flight dynamic moment balance, the hypercubic control space and the attainable moment subset at a particular flight state can be generated and analyzed. An example of the visualized attainable moment subset of the GHGV-2 at Mach 12.5 and at a constant altitude within the height band of the mesosphere is given in Fig. 8.

4.2. Control Performance Analysis

The established control performance analysis environment allows a developed FCS to be examined using time-depending variable reference signals as control commands. Furthermore, environmental influences (e.g. turbulence or gust) and failure cases can be defined within the framework. As failure cases, the control surface areas can be decreased, or even whole control effectors can be removed.
In order to additionally study the influences of model uncertainties, the control performance analysis environment was modified in a way that multiplicative parameter uncertainties in the form of EQ. 17 can be defined. For every model parameter $C_{i,j}$ defined as uncertain (please do not confuse the model parameter $C_{i,j}$ with entries of the state-space output matrix C), a maximum uncertainty spreading $\kappa_{i,j}$ around the nominal value $C_{i,j,nom}$ can be defined. The uncertainty distribution's probability density function (PDF) is invariably assumed as a Gaussian normal distribution in the current project phase. In later stages of the research activities other PDFs are considered to be added to the framework as well. As Eq. 18 displays, is the regarded uncertainty distribution factor $\Delta C_{i,j}$ defined so that the maximum occurring parameter variation will generally lie within a range of $\pm 3\sigma$ standard deviation around $C_{i,j,nom}$.

$$C_{i,j} = \Delta C_{i,j}(\kappa_{i,j}) \cdot C_{i,j,nom} \tag{17}$$

$$\Delta C_{i,j}(\kappa_{i,j}) = \mathcal{N}(\mu, \sigma^2) = \mathcal{N}(1, (\frac{\kappa_{i,j}}{3})^2) \tag{18}$$

The presented capabilities make it possible to investigate the influences of model uncertainties on the control performance within a robustness analysis using Monte Carlo simulations. It is also possible that different control architectures can be compared within the evaluation procedure. An example of a control performance comparison under the presence of uncertainties for a unit step reference on the angle-of-attack channel is displayed in Fig. 9.

5. GLIDE AND MANEUVERABILITY PERFORMANCE ASSESSMENT

One primary goal of the currently ongoing research efforts concerning hypersonic vehicles is to investigate hypersonic glide vehicles' physical limitations and performances. Concerning the previously described mission design (in Sect. 2) of the GHGV-2, it was identified that two meaningful flight performance criteria are the vehicle's glide and maneuverability performance.

5.1. Glide performance analysis

The implemented glide performance analysis for hypersonic glide vehicles is designed to evaluate and compare metrics such as the maximum glide range and glide time. The accomplished flight performance with constant (L/D) can be compared for different initial flight altitude and flight speed settings. In FIG. 10, the altitude profile over the glide range for five different flight state settings are compared. In order to not fully disclose the performance potential, it was chosen that the lift-to-drag ratio of the vehicle was fixed at the same constant value of 2.5 for each given simulation. Even though (L/D) bigger than 6 are feasible for the GHGV-2, and hence higher glide performances could be certainly achieved by the vehicle. In a further step it was assumed that the control surface deflections do not have a major impact on the overall vehicles lift-to-drag ratio and hence the influences of control deflections and losses due to the vehicle trimm were neglected.
A typical phugoid oscillation motion for a re-entry vehicle can be noticed for the simulated trajectories with higher initial velocity and altitude combinations. These motions are caused by the rapid increase of the atmospheric air density due to the decrease in altitude. Leading to a significant lift force increase since the velocity decrease during this phase is comparably slower.
The total energy of the vehicle for the simulated glide can be seen in FIG. 11. The total energy of the vehicle was computed under the consideration of both the potential and kinetic energy.
It can be observed that the total energy of the vehicle, despite minor oscillation (due to the phugoid motion), reduces nearly linearly until the system has no further energy to glide.
FIG. 12 shows the glide range development of the vehicle with respect to the glide time. It showcases how fast distances can be overcome and how short the travel time of the regarded hypersonic system is.
It can be observed that for an initial Mach number of 15 and the inital altitude of 55 km, the vehicle can glide to a distance of around 2800 km within a glide time of around 26 min. Compared to real-world dimensions, the traveled distance is equivalent to a glide over a major part of the European continent, which indicates how fast those systems can reach remote locations.

5.2. Maneuverability performance analysis

An aerial vehicle's classical maneuverability performance domains can be divided into two major classes: maneuverability and agility. Maneuverability is the measure concerning the ability of a vehicle to

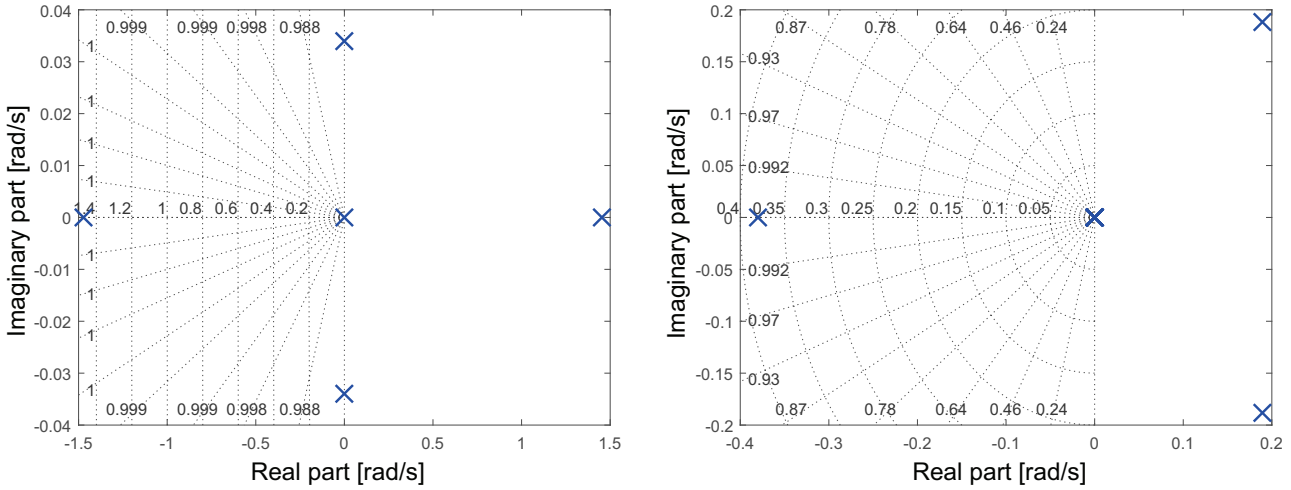

(a) Longitudinal poles **(b) Lateral-directional poles**

FIG 7. Exemplary results of the eigenvalue analysis of the linearised open-loop dynamics of the GHGV-2 at Mach 12.5 and at a constant altitude within the height band of the mesosphere

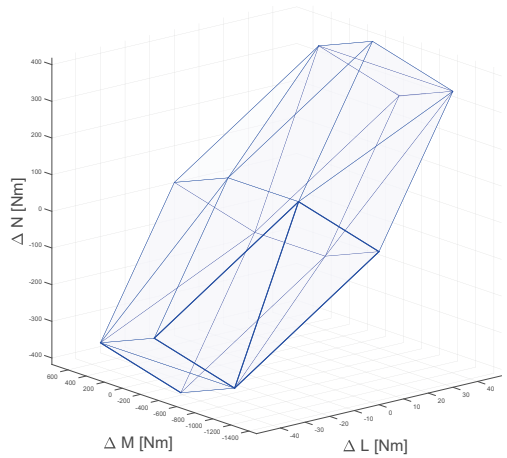

FIG 8. Exemplary visualization of the attainable moment subset of the control effectors of the GHGV-2 vehicle at Mach 12.5 and at a constant altitude within the height band of the mesosphere

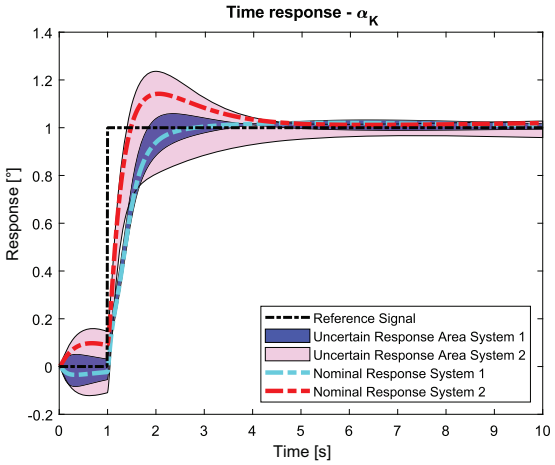

FIG 9. Monte-Carlo based comparision of two controller under the presence of uncertainty

change the aircraft flight path (velocity vector). Agility is the measure concerning the ability of a vehicle to change the aircraft acceleration vector [20].
Examples of maneuverability metrics are, for example, the maximum turn rate $\dot{\chi}_{max}$ and the minimum turn radius $R_{turn,min}$. The turn rate describes how fast a vehicle can change the heading during a level turn and can be expressed with the following equation:

$$\dot{\chi}_{max} = \frac{g\sqrt{n_z^2 - 1}}{V} \tag{19}$$

Fig. 13 shows a graph for which the turn rate of the GHGV-2 is computed for different Mach numbers at a constant altitude within the height band of the mesosphere. The computed values for each analyzed point are shown with red crosses, while the values are connected with a cubic spline displayed in black.
It can be seen that the maximum turn rate is located at a Mach number of approximately two. This maximum point is called corner velocity and is at the juncture of the aerodynamic lift limits and the structural load limits [21]. Before reaching this point, the maximum achievable lift force limits higher turn rate values of the vehicle. At Mach numbers higher than the corner velocity, the turn rate is limited by the maximum load factor $n_{z,max}$ the vehicle is allowed to achieve before structural damages would occur. The associated minimum turn radius for the analysis can be computed with the following relationship:

$$R_{turn,min} = \frac{V^2}{g\sqrt{n_z^2 - 1}} \tag{20}$$

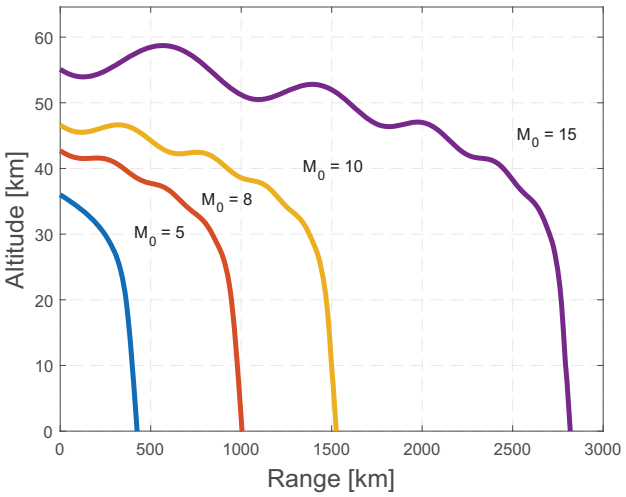

FIG 10. Altitude profile of the GHGV-2 with varying initial conditions

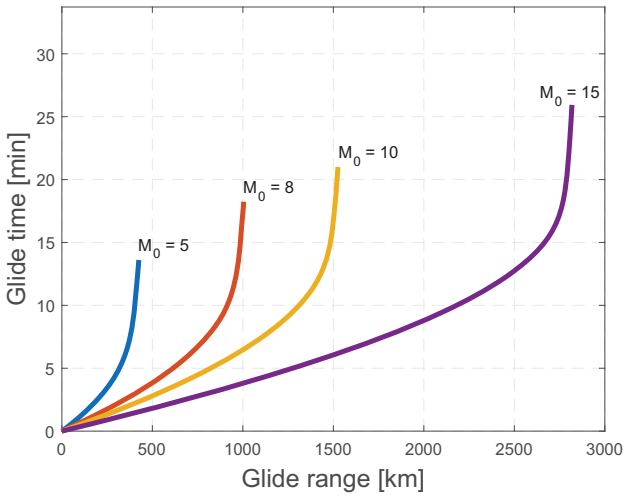

FIG 12. Glide range vs. Glide time of the GHGV-2 with varying initial conditions

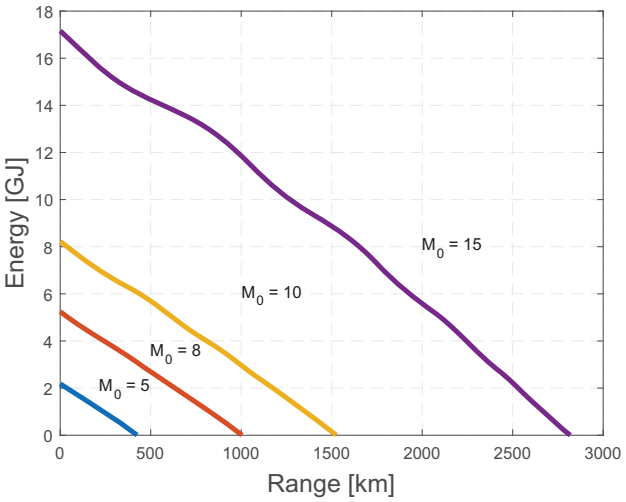

FIG 11. Energy vs. glide range of the GHGV-2 with varying initial conditions

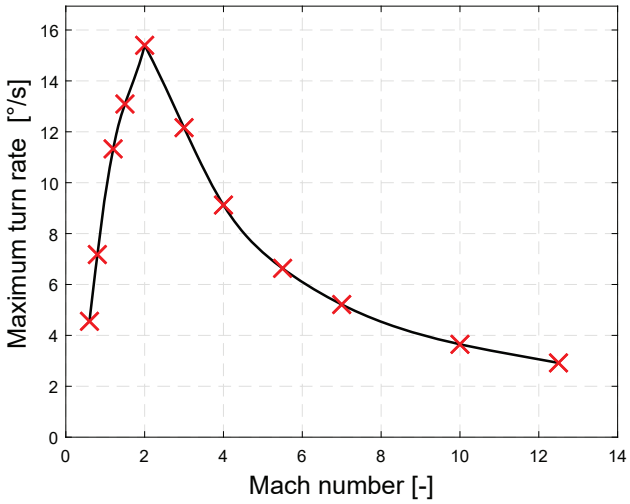

FIG 13. Maximum turn rate of the GHGV-2 for varying Mach numbers

FIG. 14 shows the GHGV-2 results for the minimum turn radius under same conditions as the priorly presented turn rate analysis.

Regarding the agility performance, the pitch and the torsional agility of the HGV were further investigated. The pitch agility analysis examines how fast the vehicle can reach a maximum achievable n_z for a particular flight state. As previously explained, the maximum achievable n_z varies depending on the flight envelope region in which the vehicle is operating. FIG. 15 shows the pitch agility analysis for the GHGV-2 for varying Mach numbers. It can be seen that pitch agility increases when the Mach number increases. However, it can be observed that the trend stops at a certain point, which is caused by the implemented control system, which was designed not to allow higher rates and consequently n_z values the system is not designed for.

A further relevant agility metric is torsional agility. The metric is defined as the ratio between the computed maximum turn rate $\dot{\chi}_{max}$ and the computed lateral agility at the same flight conditions. Lateral agility is defined as the time to roll 90° and stop while maintaining a certain angle of attack [21]. FIG. 16 shows an example of the torsional agility analysis for the GHGV-2 at at a constant altitude within the height band of the mesosphere.

6. SUMMARY

This paper presents a generic control-centric software architecture for the modeling, simulation, and analysis of conceptual hypersonic glide vehicles.

Sect. 2 showed that compared to commonly used ballistic missile systems, newly developed hypersonic operational threats are more challenging to identify and track by earth-based radar systems. Based on the regarded class of hypersonic vehicles, mission requirements, and research goals of the DLR project, it was decided to focus on four meaningful analyses classes: flight-dynamic, control-performance, maneuverability, and glide-performance.

Exemplary results for the glide and maneuverability performance analysis of the GHGV-2 were shown in

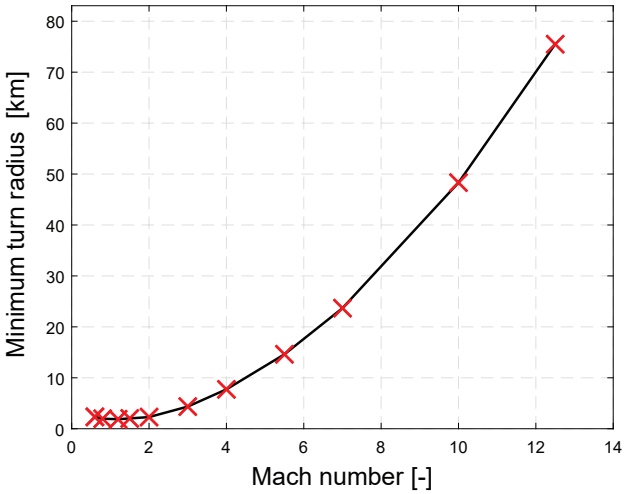

FIG 14. Minimum turn radius of the GHGV-2 for varying Mach numberss

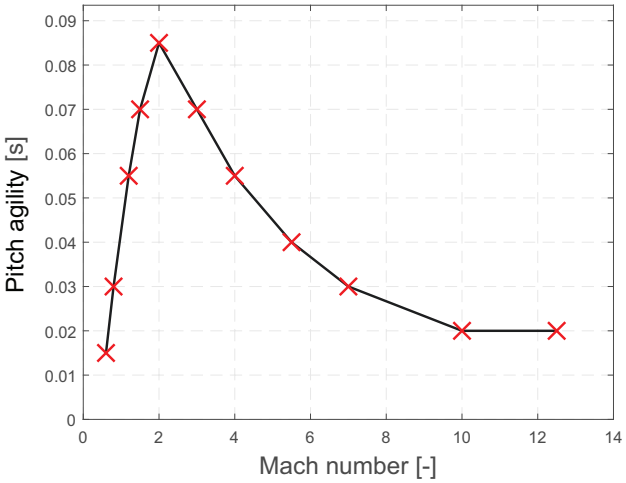

FIG 15. Pitch agility of the GHGV-2 for varying Mach numbers

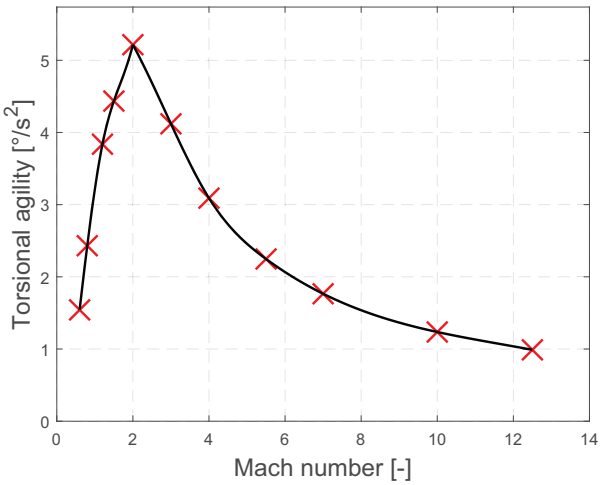

FIG 16. Torsional agility of the GHGV-2 for varying Mach numbers

Sect. 5. It was revealed how the agility properties of the GHGV-2 vary over different speed regimes and where the vehicle has its best maneuverability abilities. These results are planned to be used for the subsequent mission design and future activities with regards to the flight trajectory generation.

7. FUTURE WORK

With the goal to improve the general capabilities of the proposed simulation framework, the implemented physical model of the vehicle is planned to be enhanced. For example, the current actuator models are implemented as simplified second-order systems with acceleration, rate, and position limits. Nevertheless, high temperature and dynamic pressure conditions in hypersonic regimes can significantly impact the authority of the actuators, and hence for some cases, controllability during real-world operations cannot be fully guaranteed. In order to have a better understanding of such effects, more sophisticated and physically correct actuator models need to be implemented into the simulation. Likewise, problems are encountered for sensors and linked observability properties.
In order to further investigate the mission-oriented physical capabilities of hypersonic glide vehicles, it is intended to enhance the assessment capabilities. In future steps, it is planned to integrate methodologies that allow running realistic mission scenarios and to use the generated data to gain further knowledge of the limitations and the potential of hypersonic systems.

ACKNOWLEDGEMENT

The authors would like to thank and acknowledge all colleagues working within the HyBAB study for their contributions to the multidisciplinary design of the presented vehicle. Special thanks go to Dr. Christoph Deiler from the DLR Institute of Flight Systems for his insightful comments on the manuscript and helpful suggestions within the field of flight dynamics.

Contact address:

johannes.autenrieb@dlr.de

References

[1] Y. Liu, B. Chen, and H. Li, Y.and Shen. Overview of Control-Centric Integrated Design for Hypersonic Vehicles. *Astrodynamics*, 2(4):307–324, 2018. DOI: 10.1007/s42064-018-0027-8.

[2] A. Kelkar, J. Vogel, C. Whitmer, D. Chaussee, and C. Ford. Design Tool for Control-Centric Modeling, Analysis, and Trade Studies for Hypersonic Vehicles. In *17th AIAA International Space Planes and Hypersonic Systems and Technologies Conference 2011*, San Francisco, California, US, 04 2011. DOI: 10.2514/6.2011-2225.

[3] S. Keshmiri, R. Colgren, and M. Mirmirani. Six-Dof Modeling and Simulation of a Generic Hypersonic Vehicle, for Control and Navigation Purposes. In *AIAA Guidance, Navigation, and Control Conference and Exhibit*, Keystone, Colorado, US, April 2012. DOI: 10.2514/6.2006-6694.

[4] J. T. Parker, A. Serrani, S. Yurkovich, M. A. Bolender, and D. B. Doman. Control-Oriented Modeling of an Air-Breathing Hypersonic Vehicle. *Journal of Guidance, Control, and Dynamics*, 30(3):856–869, 2007. DOI: 10.2514/1.27830.

[5] P. R. Sudalagunta. *Control-Oriented Modeling of an Air-Breathing Hypersonic Vehicle*. PhD thesis, Virginia Polytechnic Institute and State University, Blacksburg, Virginia, US, July 2018. DOI: 10.14279/depositonce-7555.

[6] P. Gruhn. Design and Analysis of a Hypersonic Glide Vehicle (Original German Title: Auslegung und Analyse eines hypersonischen Gleitflugkörpers). In *Conference on Applied Research for Defense and Security in Germany*, Bonn, Germany, March 2020.

[7] P. Gruhn, J. Klevanski, and C. Schnepf. Flight Dynamic Simualtion of Missiles (Original German Title: Flugdynamische Simulation von Flugkörpern). In *Conference on Applied Research for Defense and Security in Germany*, Bonn, Germany, February 2018.

[8] P. Hawley and R. Blauwkamp. Six-Degree-of-Freedom Digital Simulations for Missile Guidance, Navigation, and Control. *Johns Hopkins Apl Technical Digest*, 29:71–84, 2010.

[9] T. Gerhold. Overview of the hybrid rans code tau. In N. Kroll and J. K. Fassbender, editors, *MEGAFLOW - Numerical Flow Simulation for Aircraft Design*, pages 81–92, Berlin, Heidelberg, 2005. Springer Berlin Heidelberg. DOI: 10.1007/3-540-32382-1_5.

[10] N. Fezans, D. Alazard, N. Imbert, and B. Carpentier. Robust Lpv Control Design for a RLV During Reentry. In *AIAA Guidance, Navigation, and Control Conference*, Toronto, Ontario, Canada, August 2010. DOI: 10.2514/6.2010-8194.

[11] E. Mooij. Characteristic Motion of Re-entry Vehicles. In *AIAA Atmospheric Flight Mechanics (AFM) Conference*, Boston, Massachusetts, US, August 2013. DOI: 10.2514/6.2013-4603.

[12] T. West and A. Brandis. Updated Stagnation Point Aeroheating Correlations for Mars Entry. In *2018 Joint Thermophysics and Heat Transfer Conference*, Atlanta, Georgia, US, June 2018. DOI: 10.2514/6.2018-3767.

[13] S. A. van Binsbergen, B. van Zelderen, R. G. Veraar, F. Bouquet, W. H. C. Halswijk, and H. M. A. Schleijpen. Hyperheat: A Thermal Signature Model for Super- and Hypersonic Missiles. In Karin U. Stein and Ric Schleijpen, editors, *Target and Background Signatures III*, volume 10432, pages 87 – 99. International Society for Optics and Photonics, SPIE, 2017.

[14] M. E. Tauber, G. P. Menees, and H. G. Adelman. Aerothermodynamics of Transatmospheric Vehicles. *Journal of Aircraft*, 24(9):594–602, 1987. DOI: 10.2514/3.45483.

[15] E. Rollins, J. Valasek, J. Muse, and M. Bolender. Nonlinear Adaptive Dynamic Inversion Applied to a Generic Hypersonic Vehicle. In *AIAA Guidance, Navigation, and Control (GNC) Conference, Baltimore, Massachusetts, US, August 2013*. DOI: 10.2514/6.2013-5234.

[16] M. Bolender and D. Doman. Nonlinear Longitudinal Dynamical Model of an Air-Breathing Hypersonic Vehicle. *Journal of Spacecraft and Rockets*, 44:374–387, 02 2007. DOI: 10.2514/1.23370.

[17] H. Duda, G. Bouwer, J.-M. Bauschat, and K.-U. Hahn. *A model following control approach*, pages 116–124. Springer. ISBN: 978-3-540-76151-8. December 2007. DOI: 10.1007/BFb0113855.

[18] S. A. Snell and William L. Enns, F. D.and Garrard. Nonlinear Inversion Flight Control for a Supermaneuverable Aircraft. *Journal of Guidance, Control, and Dynamics*, 15(4):976–984, 1992. DOI: 10.2514/3.20932.

[19] R. R. da Costa, Q. P. Chu, and J. A. Mulder. Reentry Flight Controller Design Using Nonlinear Dynamic Inversion. *Journal of Spacecraft and Rockets*, 40(1):64–71, 2003. DOI: 10.2514/2.3916.

[20] J. Beck and T. Cord. A Framework for Analysis of Aircraft Maneuverability. In *20th Atmospheric Flight Mechanics Conference*, Baltimore, Maryland, USA, August 1995. DOI: 10.2514/6.1995-3448.

[21] R. Liefer, J. Valasek, and D. Eggold. Fighter Agility Metrics, Research, and Test. *Journal of Aircraft*, 29, 07 1990. DOI: 10.2514/3.46182.